Environ Sci Pollut Res (2017) 24:10041–10055
DOI 10.1007/s11356-017-8410-1

Carbonaceous adsorbents derived from textile cotton waste for the removal of Alizarin S dye from aqueous effluent: kinetic and equilibrium studies

Béchir Wanassi[1,2] · Ichrak Ben Hariz[3] · Camélia Matei Ghimbeu[2] · Cyril Vaulot[2] · Mohamed Ben Hassen[1,4] · Mejdi Jeguirim[2]

Received: 21 June 2016 / Accepted: 5 January 2017 / Published online: 27 January 2017

Abstract Recycling cotton waste derived from the textile industry was used as a low-cost precursor for the elaboration of an activated carbon (AC) through carbonization and zinc chloride chemical activation. The AC morphological, textural, and surface chemistry properties were determined using different analytical techniques including Fourier transform infrared, temperature programmed desorption-mass spectroscopy, nitrogen manometry and scanning electron microscopy. The results show that the AC was with a hollow fiber structure in an apparent diameter of about 6.5 μm. These analyses indicate that the AC is microporous and present a uniform pore size distributed centered around 1 nm. The surface area and micropore volume were 292 $m^2.g^{-1}$ and 0.11 $cm^3.g^{-1}$, respectively. Several types of acidic and basic oxygenated surface groups were highlighted. The point of zero charge (pH_{PZC}) of theca was 6.8. The AC performance was evaluated for the removal of Alizarin Red S (ARS) from aqueous solution. The maximum adsorption capacity was 74 $mg.g^{-1}$ obtained at 25 °C and pH = 3. Kinetics and equilibrium models were used to determine the interaction nature of the ARS with the AC. Statistical tools were used to select the suitable models. The pseudo-second order was found to be the most appropriate kinetic model. The application of two and three isotherm models shows that Langmuir–Freundlich (n = 0.84, K = 0.0014 $L.mg^{-1}$, and q = 250 $mg.g^{-1}$) and Sips (n = 0.84, K = 0.003 $L.mg^{-1}$, and q = 232.6 $mg.g^{-1}$) were the suitable models. The results demonstrated that cotton waste can be used in the textile industry as a low-cost precursor for the AC synthesis and the removal of anionic dye from textile wastewater.

Keywords Recycling cotton waste · Activated carbon · Characterization · Textile effluent treatment · Alizarin Red S

Responsible editor: Philippe Garrigues

✉ Mejdi Jeguirim
mejdi.jeguirim@uha.fr

[1] Laboratoire du Génie Textile, LGTex, Université de Monastir, 5078 Ksar Hellal, Tunisie

[2] Institut de Science des Matériaux de Mulhouse, UMR 7361 CNRS, UHA, 15, rue Jean-Starcky, 68057 Mulhouse, France

[3] Société Tunisienne des Industries de Raffinage, P8, Zarzouna, Tunisia

[4] College of Engineering: Industrial Engineering Department, Taibah University, Medina, Saudi Arabia

Introduction

The development of the textile industries has been accompanied by the generation of huge quantities of solid wastes and wastewater effluents. Approximately, 10^6 tons of textiles solid wastes are annually produced worldwide (Ouchi et al. 2010) and this amount is continuously increasing every year due to the increasing number of fashion seasons (Ali and Courtenay 2014). Environmental pollution due to the textile effluents is a major problem because of their toxicities and harmful effects on the environment and health. Annually, 10 to 15 10^4 tons of dyes are released into the environment (Foo and Hameed 2010; Gupta and Suhas 2009). During the textile dye process, 2–20% of dyes are lost in wastewater effluents generating a severe risk to the aquatic system (Zaharia and Suteu 2012). In addition, these effluents can cause toxic, carcinogenic, and mutagenic effects on animals and human health (Almasian et al. 2015).

In the last decades, several technologies have been investigated for the decolorization of textile effluents. These techniques could be divided into three kinds of treatment, namely,

biological, dielectric, and physical treatments. Biological textile effluent treatment was widely used in the textile industry. This technique was considered as low cost and high removal efficient. However, this technique is very slow and depends strongly on several factors such as pH effluent (Zahid et al. 2016; Dongqing et al. 2016). Dielectrical approach has been also applied in textile wastewater treatment (Mouele et al. 2015) due to its efficiency to decrease the toxicity of textile effluents to a near zero value. In addition, dielectrical process has the advantage to be a low-cost energy process and moreover requests short decolorization time. However, such technology leads to the generation of ozone and UV radiation which may be regarded as an important inconvenience (Martynas et al. 2013).

The physical treatment (adsorption) using activated carbon (AC) (Gupta et al. 2011) seems to be the most promising technique for the decolorization of textile effluents. Several investigations have privileged the use of low-cost precursor such as lignocellulosic biomass for the production of efficient activated carbons. Among these precursors, *Luffa cylindrica* fibers (Kesraoui et al. 2015), *Agave americana* fibers (Ben Hamissa et al. 2010), and *Posidonia oceanica* fibers (Ncibi et al. 2006) were used to develop activated carbon for textile effluent treatment.

Cotton fiber is the most lignocellulosic and the noblest fiber used worldwide. Recycling cotton waste can be considered as a good and low-cost resource for lignocellulosic materials. In order to overcome the economic and environmental impact of cotton waste, to give an added value and a second life should be clearly considered. Haule and Carr (2016) and Haule et al. (2014) studied the supramolecular and accessibility properties of the cellulosic fibers regenerated from cotton waste garments. The mechanical and physical properties of the regenerated fibers were found to be more interesting than traditional lyocell fibers. Jie et al. (2016) evaluated the opportunity to use waste cotton fabrics for the manufacturing of water-soluble cellulose acetate. Results revealed that bio-based cellulose composites can be made-up by aqueous blending of the obtained cellulose acetate and two kinds of nanocelluloses (cellulose nanocrystals and cellulose nanofibrils). The obtained material can be used in packaging, sheet coating and binders, etc. Zainab and Ali (2016) investigated at a laboratory scale the recycling of medical cotton industry wastes for biogas production using the anaerobic digestion procedure. Results revealed that the biogas maximum yield was 92% in optimum condition of temperature, pretreatment of substrate, and addition of inoculums.

Few studies have used the cotton fiber waste as a precursor for activated carbon elaboration. This valorization strategy is very interesting since an activated carbon prepared from textile industry waste could be used locally for the treatment of textile wastewater effluents. Jieying et al. (2014) employed cotton-woven waste for activated carbon production. In the optimum condition of temperature, carbonization and activation times (800 °C-30 min and 700 °C-30 min, respectively), the obtained surface area was 789 $m^2.g^{-1}$ and the iodine value was 1147 $mg.g^{-1}$. Such derived carbon was successfully used to remove more than 80% of the chemical oxygen demand (COD) from oilfield wastewater.

Ekrami et al. (2014) optimized the preparation of activated carbon derived from waste cotton fiber using the chemical activation method with phosphoric acid. The preparation-optimized conditions of AC were the following: activation temperature 450 °C, time of activation 30 min, impregnation ratio of 2 wt.% the S_{BET} (BET surface area), and the average pore diameter of the obtained AC were 494 $m^2.g^{-1}$ and 1.91 nm, respectively. These textural properties may influence the adsorption of molecules from aqueous solutions.

In textile dyeing industry, several types of dye were used such as anionic, cationic, and pigment dye. The most research works on the decolorization of textile effluents have examined essentially the adsorption of methylene blue (MB) in spite availability of different dyes. Among the various dyes, Alizarin (ARS, $C_{14}H_7NaO_7S$, H_2O), a red pigment of plant origin, extracted from the root of the Dyers Madder (*Rubia tinctorum* L.), is widely used in textile industry (Javad et al. 2014; Parra et al. 2004). This dye belongs to the family of hazard pollutants which require a post treatment technique in order to avoid its discharge in the environment.

In a previous study, a recycling process of cotton waste yarn from the Society of Textile Industry (SITEX, Tunisia) was implemented (Wanassi et al. 2016). Reclaimed fibers were used to spin blended cotton yarn. Around 20% of these fibers cannot be used for spinning because of their poor mechanical and physical properties. Therefore, it seems necessary to give an added value to these cotton waste fibers. Hence, the main purpose of this study is to synthesize an activated carbon from these fibers. This activated carbon could be used locally in the industrial plant for textile effluent treatment. Thus, the performance of the elaborated carbonaceous adsorbent is evaluated for the removal of Alizarin from aqueous solution. Several kinetics and isotherm models as well as thermodynamic calculations are used to understand the interaction nature between the activated carbon and the Alizarin dye. These calculations are supported by statistical tools in order to select the suitable models and to extract the required parameters for the design of effluent treatment plant.

Materials and methods

Raw materials

The precursor used in this study was the waste generated by the recycling of cotton fibers (Wanassi et al. 2016) in the textile industry company SITEX (Société Industrielle de

Textile, Ksar Hellal, Tunisia). These residual fibers are not valorized currently since they cannot be used for spinning due to their poor technical characteristics (mean length 18.5 mm, tenacity 28.3 cN/Tex). The SITEX company is committed to reduce its environmental impact through water consumption reduction, efficient wastewater treatment, and waste minimization. Therefore, the recovery of cotton fibers through activated carbon elaboration is proposed in this present investigation.

Activated carbon preparation

Prior to the preparation of the activated carbon, the cotton fibers were washed with distilled water and dried at 105 °C during 48 h. Then, 10 g of cotton fibers were pyrolysed in a horizontal tubular furnace under 25-mL/min argon rate from room temperature to 700 °C with a 5 °C/min heating rate. The sample was kept at 700 °C during 1 h and then cooled to room temperature. After that, the pyrolysed cotton fibers were activated chemically through immersion in zinc chloride solution (20% *w*/*w*) at room temperature for 24 h. After impregnation, the sample was filtered, washed, and dried in an oven at 105 °C.

Cotton fibers and activated carbon characterizations

The raw materials as well as the elaborated activated carbon were characterized using different analytical techniques.

The thermal degradation behavior of the cotton fibers under inert atmosphere was examined using thermogravimetric analyzer (METTLER-TOLEDO TGA 851e). During thermogravimetric analyzer (TGA) run, 5 mg of cotton fibers were placed in an alumina crucible. TGA experiments were performed under nitrogen gas flow at heating rates of 5 °C/min from room temperature to 800 °C.

The activated carbon morphology was characterized by scanning electron microscopy (Philips model FEI model Quanta 400 SEM). The AC textural properties were characterized by measuring nitrogen adsorption isotherms at 77 K using a Micromeritics (ASAP 2020) gas adsorption analyzer. Before the analysis, the sample was out-gassed overnight in vacuum at 623 K. The BET (Brunauer–Emmett–Teller) surface area (S_{BET}) of AC was calculated from N_2 adsorption isotherms in relative pressure (P/P_0) range of 0.05–0.30. The micropore surface (S_{mic}) area and the micropore volume (V_{micro}) were explored from *t*-plot method.

The characterization of AC surface chemistry was carried out using Fourier transform infrared spectroscopy (FTIR) and temperature programmed desorption-mass spectroscopy (TPD-MS). The functional groups on the AC surface were evaluated using Jasco FTIR 4100 series spectrophotometer (manufactured by PIKE Technologies). The spectra were obtained with a resolution of 4 cm^{-1} using 64 cumulative scans. The spectra were recorded from 4000 to 600 cm^{-1}. The cotton fibers were also examined using FTIR analysis in order to evaluate the effect of the carbonization and the activation on the surface chemistry evolution

Quantitative and qualitative information on the functionalities of the AC surface was assessed using TPD-MS analysis. During this analysis, 5 mg of AC was deposited in a quartz tube in a furnace and heat treated from room temperature to 900 °C with 5 °C.min^{-1} heating rate in vacuum. During the experiment, mass spectrometer analyzed continuously the evolved gas. From the TPD analysis, desorption rate of each gas (H_2, H_2O, CO, and CO_2) as a function of temperature was determined. By time integration of TPD-MS peaks, the quantities of released gas were as well determined.

Adsorption tests

Alizarin Red S (ARS) used in this study was purchased from Sigma Aldrich, UK. The dye solutions were prepared by dissolving an appropriate amount of dye in distilled water. In a typical experiment, 5 mg of activated carbon was placed in 10-mL aqueous solution of dye and the adsorption tests were conducted at a constant agitation speed of 200 rpm using a shaking thermostat water bath. The influence of the operating conditions on the removal of ARS was examined through the variation of the initial dye concentration in water (5–200 mg.L^{-1}), the pH of solution (3–8), the contact time (5–1440 min) and the solution temperature (18–40 °C). The ARS concentration was determined by using a double beam UV-visible spectrophotometer.

The adsorption capacity of ARS by activated carbon was determined as follows:

$$q\left(\mathrm{mg.g^{-1}}\right) = \frac{C_i - C_e}{M} \times V$$

Where q (mg.g^{-1}) is the quantity of ARS adsorbed, C_i (mg.L^{-1}) is the initial ARS concentration, C_e (mg.L^{-1}) is the equilibrium ARS concentration and V (L) initial ARS solution volume and M (g) is the mass of adsorbent.

Mathematical approach

Different kinetic and equilibrium models as well as thermodynamic calculations were used to analyze the nature of the interactions of ARS with the activated carbon.

Kinetic models

Pseudo first-order, pseudo second-order, and intra-particular diffusion models were evaluated to describe the ARS adsorption kinetics. The linear forms of each model are presented in Table 1. Where k_1 was the rate constant of pseudo-first order

Table 1 Kinetic models

Model	Equation	Reference
Pseudo-first order	$\log(q_e - q_t) = \log(q_e) - \frac{k_1}{2.303} t$	(Lagergren 1998)
Pseudo-second order	$\frac{t}{q_t} = \frac{1}{k_2 q^2_{eq}} + \frac{t}{q^2_{eq}}$	(Ho and McKay 1999)
External diffusion	$\ln \frac{C_0 - C_e}{C_t - C_e} = K.\frac{a}{V}.t = K'.t$	(Mehrorang et al. 2012)
Intra-particular diffusion	$q_t = K_{id}.t^{\frac{1}{2}} + C$	(Kumar and Smaïl 2010)

(min^{-1}), k_2 was the rate constant of pseudo-second order ($L.mg^{-1}.min^{-1}$), K' was the constant of external diffusion (min^{-1}), and k_{id} was the constant of intra-particular diffusion ($mL^{-1}.min^{-1/2}$).

Equilibrium models

In order to identify the ARS adsorption isotherm, different two-parameter and three-parameter isotherm models were tested. The isotherm parameter determination contributes to the understanding of the adsorbent surface heterogeneity and lateral interactions (Koopal et al. 1994) that may exist between the ARS and the AC.

The linear forms of the two- and three-parameter models are shown in Table 2. For the three-parameter models, the application of linear regression on the linear form could not allow to extract the different parameters. Hence, a specific procedure including two steps was used to determine the isotherm parameter value. The first step was to test the non-linear models using non-linear regression algorithms (ORIGIN LAB 8.5.1 software). The second step was to use one value from the three parameters (K_L, q_m, or n from the non-linear model) into the linear model, which converts into a two-parameter model that can be linearized. Generally, the linear forms of three-parameter models were based on the supposition that n value is known.

Statistical approach

Linear and non-linear regression of the experimental and calculated isotherm data were performed by minimizing the residual sum of square (RSS) value. It is a measurement of the difference between the experimental and calculated data. The RSS value was calculated according to:

$$\mathrm{RSS} = \sum_{i=1}^{n} \left(Y^i_{\mathrm{exp}} - Y^i_{\mathrm{th}} \right)^2$$

Where Y_{exp} and Y_{th} were, respectively, the experimental and calculated values and n was the number of experimental values.

The predictive performance of kinetics, thermodynamic, and isotherm models was, firstly, examined by regressing models using R^2 statistic value. High value of R^2 (>0.97) indicates that each models may be ranked accordingly, and vice versa. R^2 was calculated with this following equation:

$$R^2 = 1 - \frac{\sum_{i=1}^{n} \left(y_i - \hat{y}_1 \right)^2}{\sum_{i=1}^{n} \left(y_i - \overline{y}_1 \right)^2}$$

Where y_i was the experimental value, $\hat{y}_1$was the calculated value, and $\overline{y_i}$ was the mean value.

The majority of the previous study used only R^2 to select the most adequate model. In this study, more statistical parameters (F_{calc} and P value) have been used in order to minimize the error interval. F_{calc} was calculated with the following equation:

$$F_{\mathrm{calc}} = \frac{(n-1)\sum \left(q^{\mathrm{exp}}_{\mathrm{e,i}} - \overline{q}^{\mathrm{exp}}_{\mathrm{e}} \right)^2}{(n-1)\sum \left(q^{\mathrm{exp}}_{e,i} - q^{t}_{e,i} \right)^2}$$

Where i was the number of adjusted parameters of the models and $\overline{q}^{\mathrm{exp}}_e$ was the mean value of q^{exp}_e.

The P value was defined as the probability of obtaining a calculated result equal to experimental value. If P value was less than 0.05, the tested model can be considered statistically significant, and vice versa. In this study, P value was calculated using ORGINLAB 8.5 software.

Results and discussion

Raw cotton fibers and activated carbon characterizations

TGA and DTG curves of the waste recycled from cotton fibers during the thermal degradation under inert atmosphere are shown in Fig. 1.

DTG curve exhibits three main degradation zones. The first zone (<400 K) involved the removal of water content in the fiber (4.5%) and some reorganization of the cellulose arrangement (Gurudatt et al. 1999). In the second zone (370–640 K),

Table 2 Two- and three-parameter isotherm models

Model	Equation	Linear form	Reference
Two-parameter models			
Langmuir	$q_e = \frac{q_m.K_L.C_e}{1+K_L.C_e}$	$\frac{C_e}{q_e} = \frac{1}{q_m}.C_e + \frac{1}{K_L.q_m}$	(Langmuir 1918)
Freundlich	$q_e = K_F.C_e^{\frac{1}{n}}$	$\log(q_e) = \log(K_F) + \frac{1}{n}.\log(C_e)$	(Freundlich 1906)
Dubinin–Radushkevich	$\frac{q_e}{q_{mDR}} = \exp(-\beta\varepsilon^2)$	$\ln(q_e) = \ln(q_{mDR}) - \left(\frac{RT}{E}\right)^2.\left(\ln\left(\frac{C_s}{C_e}\right)^2\right)$	(Dubinin 1960)
Three-parameter models			
Redlich–Peterson	$\frac{q_e}{q_m} = \frac{K_L C_e}{1+(K_L C_e)^n}$	$\frac{C_e}{q_e} = \frac{1}{K_L q_m} + \frac{K_L^{(n-1)}}{q_m}.(C_e)^n$	(Redlich and Peterson 1959)
Tóth	$\frac{q_e}{q_m} = \frac{K_L.C_e}{[1+(K_L.C_e)^n]^{1/n}}$	$\left(\frac{C_e}{q_e}\right)^n = \left(\frac{1}{q_m.K_L}\right)^n + \left(\frac{1}{q_m}\right)^n.(C_e)^n$	(Gimbert et al. 2008)
Languir–Freundlich	$\frac{q_e}{q_m} = \frac{(K_L C_e)^n}{1+(K_L C_e)^n}$	$\frac{q_m}{q_e} = 1 + \frac{1}{(K_L C_e)^n}$	(Hinz 2001)
Langmuir general	$\frac{q_e}{q_m} = \left[\frac{K_L C_e}{1+(K_L C_e)}\right]^n$	$\left(\frac{q_m}{q_e}\right)^{\frac{1}{n}} = 1 + \frac{1}{K_G C_e}$	(Hinz 2001)
Sips	$\frac{q_e}{q_m} = \frac{K_S C_e^n}{1+K_S C_e^n}$	$\frac{1}{q_e} = \frac{1}{q_m} + \frac{1}{K_L q_m C_e^n}$	(Sips 1948)
Radke–Prausnitz 1	$\frac{q_e}{q_m} = \frac{K_L.C_e}{(1+K_L.C_e)^n}$	$\left(\frac{C_e}{q_e}\right)^{\frac{1}{n}} = \left(\frac{1}{q_m.K_L}\right)^{\frac{1}{n}} + \frac{C_e(K_L)^{\frac{n-1}{n}}}{q_m^{\frac{1}{n}}}$	(Radke and Prausnitz 1972)
Radke–Prausnitz 2	$\frac{q_e}{q_m} = \frac{K_L.C_e}{1+K_L.(C_e)^n}$	$\frac{C_e}{q_e} = \left(\frac{1}{q_m.K_L}\right) + \frac{(C_e)^n}{q_m}$	
Radke–Prausnitz 3	$\frac{q_e}{q_m} = \frac{K_L.C_e^n}{1+K_L.(C_e)^{(n-1)}}$	$\frac{C_e}{q_e} = \left(\frac{(C_e)^{1-n}}{q_m.K_L}\right) + \frac{1}{q_m}$	
Fritz–Schluender	$\frac{q_e}{q_m} = \frac{K_L.C_e}{1+q_{mFS}.(C_e)^n}$	$\frac{C_e}{q_e} = \left(\frac{1}{q_m.K_L}\right) + \frac{(C_e)^n}{K_L}$	(Fritz and Schluender 1974)

there is a considerable decrease in weight loss. At this stage, the mass loss is highly related to the thermal degradation of cellulose and hemicellulose as the main components of cotton fiber (≈90%) (Loelovich 2008). On the other hand, there is a production of tars, water, carbon monoxide, and carbon dioxide (Pastor et al. 1999). The third zone in the region of 650 to 750 K involved the degradation of lignin, and the rate of weight loss of lignin is very slow compared to that of cellulose

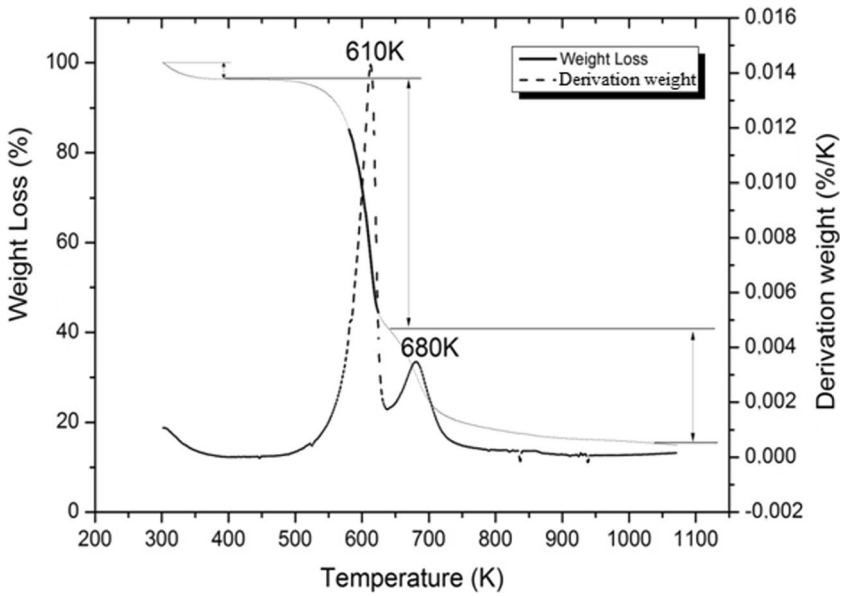

Fig. 1 Thermogravimetric analysis of waste cotton fiber

and hemicellulose. According to a previous work (Antal, 1984), a thermal degradation of a lignin is accompanied by the formation of H_2O, CO, and CO_2.

SEM analysis was used to evaluate the effect of carbonization and the chemical activation on the morphological evolution of the cotton waste. Indeed, as shown in Fig. 2, the morphology of the raw cotton fiber surface was radically changed after the thermal and chemical treatment. Firstly, appearance of a cavity core inside the fiber after the treatment is clearly noted (Fig. 2c). Secondly, a porous structure on the AC surface is observed. The chemical treatment attacks the external layer of the cotton fiber which is principally formed by the lignin. Modification in fiber diameter is noticed as well; the raw cotton fiber diameter was 13.5 μm (cv = 21%) and decreases by 50% (diameter of AC fibers 6.5 μm, cv = 9%) after carbonization and chemical treatment. The fibrils of the carbonized cellulose are noticeably revealed on the surface of the fiber with a thin layer of lignin randomly distributed on the surface of micro fibril (Fig. 2d).

FTIR analysis was used to analyze the surface groups on the cotton waste and the elaborated AC (Fig. 3). Different functional groups were identified during this analytical technique. The cotton waste fibers contained supplementary bands compared to the prepared activated carbon which is expected after a thermal treatment at 700 °C. The main peaks in the spectra of cotton waste fiber are related to O–H stretching vibration and asymmetric C–H stretching (in methylene groups), The main peaks in the spectra of cotton waste fiber are related to O–H stretching vibration, asymmetric C–H stretching (in methylene groups), –C = O, C = C–COO–, and C = C stretching vibration at 3433 cm^{-1} (Li et al. 2007; Liang et al. 2010), 2936 cm^{-1} (Altıntıg et al., 2016), 1730 cm^{-1} (Tzvetkov et al., 2016), 1530 cm^{-1} (Liou, 2010 ; Nasiri Azad et al., 2015), and 1230 cm^{-1} (Guo and Rockstraw, 2006), respectively. The important peak at 3433 cm^{-1} (O–H stretching vibration) corresponds to alcohols, phenols, and carboxylic acids existing in pectin, cellulose, and lignin respectively (Li et al. 2007; Liang et al. 2010). After thermal and chemical treatments, the surface chemical structure was modified. Indeed, the removal of high amounts of functional groups is demonstrated by the disappearance of several peaks placed initially between 3500 and 1600 cm^{-1}. The intense reduction of the band at 2936 cm^{-1} assigned to asymmetric C–H stretching indicates that the chemical activation removes a significant amount of hydrogen as well. On the other hand, it can be seen as an appearance of new peaks in the bands located in a range between 1800 and 600 cm^{-1} due to C–C, C = C aromatic and carboxylic anhydrides C–H stretching.

Surface chemistry of activated carbon was analyzed using TPD-MS technique. While the IR provides information of the existing groups in the surface of the materials, the TPD-MS gives information about the whole material and in addition, it allows quantifying the groups. By heating the AC under vacuum, the surface groups are decomposed mainly in CO, CO_2, H_2O, and H_2. The TPD-MS desorption peaks can be therefore assigned to the different surface groups on AC by comparison with similar materials in literature.

Figure 4 shows the CO_2, CO, and H_2O desorption profile of AC from 25 to 900 °C. CO_2 desorption curves of AC show two peaks at 350 and 580 °C. Desorption of CO_2 obtained at 350 °C corresponds to the presence of carboxylic groups, whereas that observed at 580 °C could be typical of anhydride or lactones. According to previous studies (Otake and Jenkins, 1993; Marchon et al. 1988, Ghouma et al. 2015), desorption of

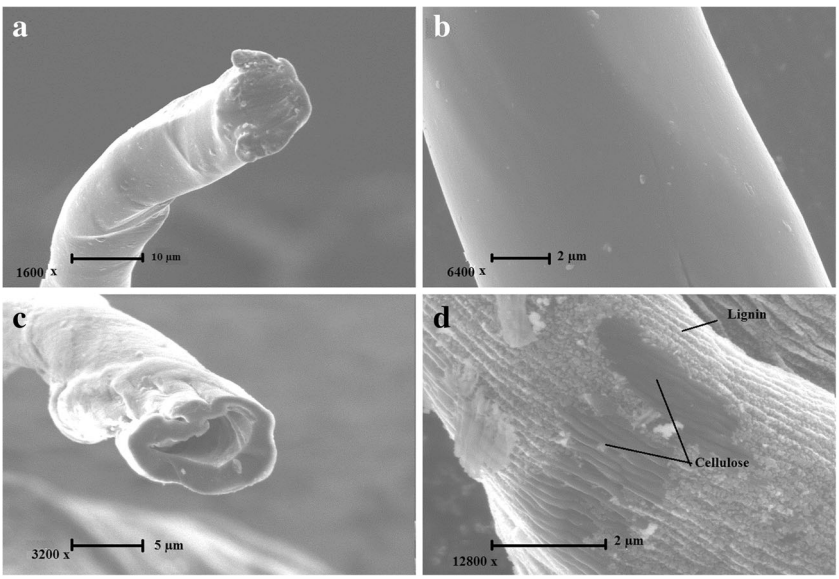

Fig. 2 SEM pictures of raw cotton (**a**, **b**) and activated carbon (**c**, **d**)

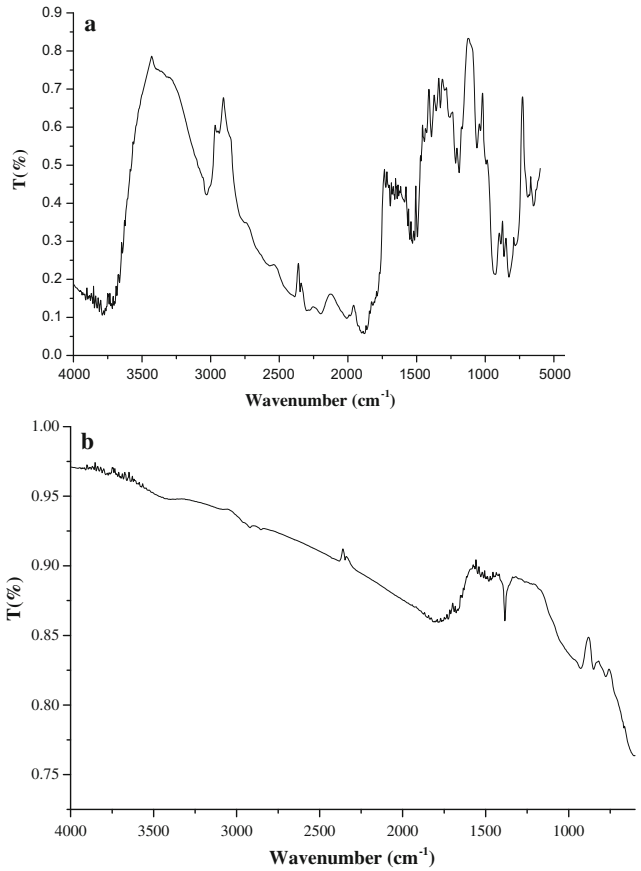

Fig. 3 FTIR analysis of **a** raw cotton and **b** the activated carbon

CO_2 at low temperature indicates the decomposition of acidic groups from lactone and carboxylic while at high temperature, it was due to the decomposition of anhydride groups (Zhuang et al. 1994).

TPD-MS profile for H_2O exhibits three desorption peaks at 200, 350, and 650 °C, respectively. The water desorption at 200 °C can be assigned to physisorbed water. The desorption peaks at 350 and 650 °C could be attributed to the in situ dehydration of carboxylic and phenolic groups which give anhydrides, lactones, and ethers.

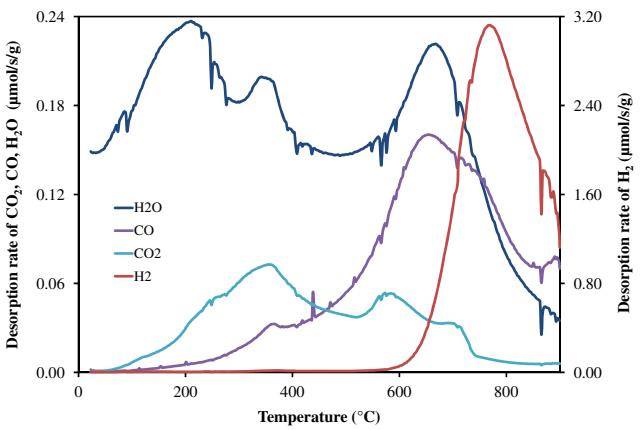

Fig. 4 TPD-MS desorption curves of the activated carbon

CO desorption rate increases with temperature and presents a peak at 650 °C. Desorption of CO is attributed to the decomposition of neutral or basic groups, such as ether, quinone, phenol, and carbonyls groups. Otherwise, a great peak of hydrogen is observed at 760 °C which is typical for the cleavage of the C–H bonds.

Total quantity of H_2, H_2O, CO, and CO_2 emitted gases was obtained from the integration of desorption peaks between 25 and 950 °C. The obtained results are shown in Table 3. The obtained values show that the amount of CO is two times higher than the amount of CO_2; hence, the materials are rather basic in nature. Such behavior was already obtained for an activated carbon prepared from the zinc chloride activation of date stone (Belhechemi et al., 2014). Authors obtained 0.53 mmol.$g^{-1}$for CO and 0.21 mmol.g^{-1} for CO_2.

Nitrogen isotherm at 77 K was used to characterize the textural features of the synthesized activated carbon AC, i.e., the specific surface area and pore structure (Fig. 5). A type I isotherm is characterizing the materials which is specific to microporous materials. The profile is the result of unrestricted monolayer–multilayer adsorption up to high value of p/p_0.

The DFT pore size distribution provided in Fig. 5b shows a well-defined peak suggesting uniform pores centered around 1 nm and also some pores with sizes higher than 2 nm can be noticed.

The textural properties of the elaborated activated carbon are the following: BET surface area S_{BET} = 292 $m^2.g^{-1}$, micropore surface S_{mic} = 255 $m^2.g^{-1}$, mesopore volume V_{meso} = 0.03 $cm^3.g^{-1}$, micropore volume V_{mic} = 0.11 $cm^3.g^{-1}$, total pore volume V_t = 0.14 $cm^3.g^{-1}$, and average pore diameter D_p = 1.96 nm. The V_{mic}/V_t ratio in the prepared AC was 76%, which indicates that the prepared AC is microporous with the presence of some mesoporosity. The specific surface was lower than the values obtained with similar precursor. This difference is attributed to the AC-selected synthesis protocol. In fact, a soft treatment was used in preparation of the activated carbon (zinc chloride, ambient temperature) in order to keep the surface structure of the initial product as shown in Fig. 6. This structure will help the elaboration of a filter to be used at a large scale. The use of other protocols may be interesting to improve the textural properties but may damage the precursor structure. As an example, Jieying et al. (2014) used a protocol leading to the

Table 3 Total quantity of released gases

Gas	mmol.g^{-1}
H_2	6.57
H_2O	1.73
CO	0.64
CO_2	0.34

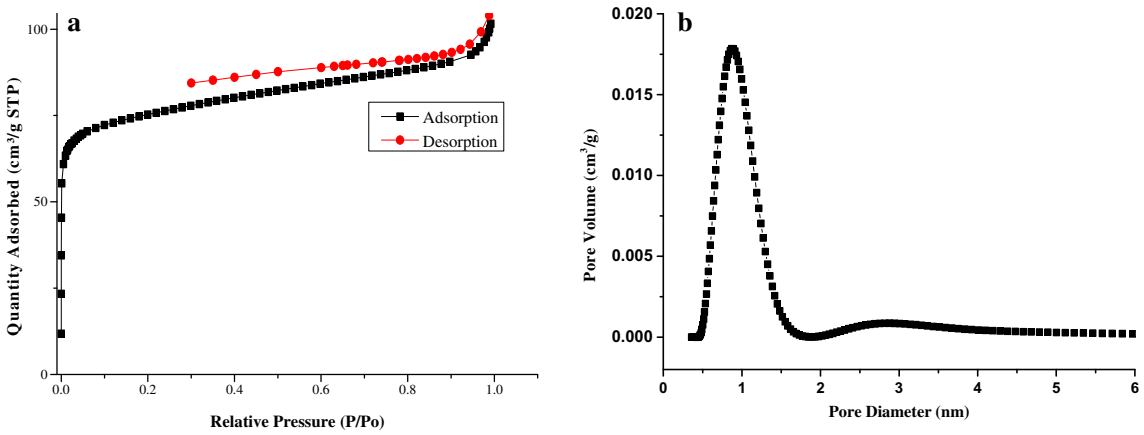

Fig. 5 **a** Nitrogen adsorption isotherm and **b** DFT pore size distribution of activated carbon

preparation of an activated carbon from cotton tissue with high specific surface area (789 $m^2.g^{-1}$). However, a lower yield of activated carbon in the pulp shape was obtained.

Effect of the pH on the AC adsorption capacity

In order to optimize the operating conditions for the ARS adsorption, the influence of solution pH was examined. Hence, four dye solutions were prepared using the following initial pH: 3, 5, 6, and 8. The pH of the initial solution was adjusted with the concentrated solution of sodium hydroxide (NaOH) (1 M) to do basic pH solution or hydro chloric acid (HCl) (89%) to do acid pH solution. The experimental conditions were as follows: adsorbent weight 5 mg, solution volume 10 mL, contact time 1440 min, stirring 200 rpm, controlled temperature 25 °C, and initial concentration 100 $mg.L^{-1}$.

Figure 7 shows the adsorption capacities vs the solution pH. It can be seen that when the initial pH increases, from 3 to 8, the adsorption capacity of the AC decreases. In the same way, the adsorption capacity decreases from 57.2 to 8.7 $mg.g^{-1}$ when the pH of the solution increases from 3 to 8. This result may be accounted to the deprotonation (Deprotonation is a chemical reaction at which a proton H^+ is removed from a molecule which forms its conjugate base.)

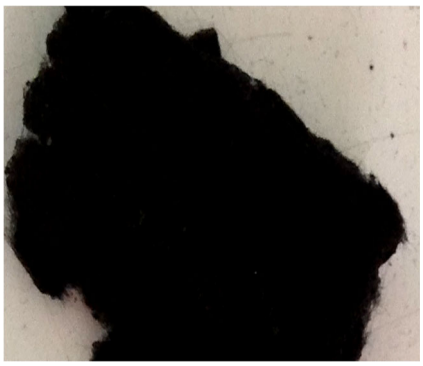

Fig. 6 Surface structure of obtained AC

of the surface of the adsorbent and the positive charges in the surface of AC which react with the alizarin that exists under the monoanionic form.

The initial pH of the ARS solution has a significant effect on the surface chemistry of the adsorbent which affects significantly the electrostatic charges that were transmitted by ionic dye molecules. The ARS adsorption was highly dependent on the pH of the solution due to the existence of several functional groups distributed on the surface of AC such as hydroxyl and carbonyl groups. Similar results were shown during the adsorption of anionic dyes by activated carbons (Pirillo et al. 2009; Sylvie et al. 2005; Azquez et al., 2014).

The pH of point charge zero (pH_{pzc}) of adsorbents is a very important parameter which can identify the potential of the interaction between the functional groups in the interface adsorbent/adsorbate in aqueous solution. ARS is an acid dye, its dissolution in water releasing negatively charged colored ions (anions). Generally, the AC surface is negatively charged where pH values were greater than those of pH_{pzc} and positively charged when pH values were lower than those of pH_{pzc} (Bazrafshan et al., 2015). At pH of ARS solution lower than pH_{pzc}, the AC surface is positively charged which strongly favors the attraction of ARS (anionic dye). The adsorption capacity of ARS by AC is maximized at an initial pH of solution less than pH_{pzc} of the AC.

Effect of initial concentration on the adsorption capacity

In order to study the impact of the initial concentration on the adsorbed quantity, eight solutions were prepared with different concentrations comprised between 10 and 300 $mg.L^{-1}$.

According to Fig. 8, the adsorption capacity increases with the increasing of the ARS initial concentration from 9 to 78 $mg.g^{-1}$ when the initial concentration increases from 10 to 300 $mg.l^{-1}$. The initial concentration generates an important force having an effect on dye mass transfer resistance between the aqueous phase and the solid phases.

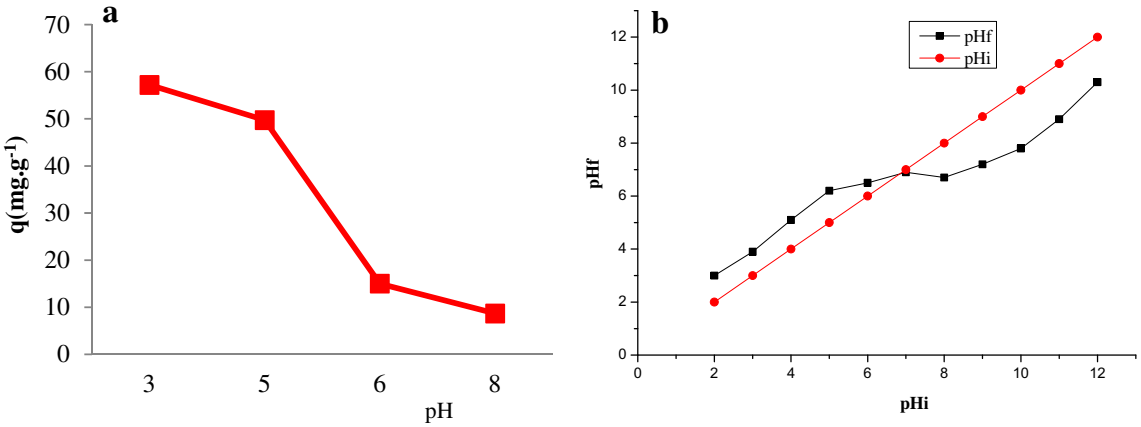

Fig. 7 **a** Influence of the solution pH on the adsorption capacity. **b** pHpzc of activated carbon (25 °C, 100 mg L^{-1}, 1440 h)

Effect of contact time on the adsorption capacity

The effect of contact time was also examined. Figure 9 shows that the curve of q vs time is composed by two phases. The first phase occurs up to 300 min and is characterized by a rapid and sharp ARS adsorbed quantity. The second phase is characterized by a slow adsorption capacity until the equilibrium after 1440 min. During the first stage, the sites are occupied progressively when the ARS tends to move to the pore in the AC surface. This adsorption phenomenon (rapid diffusion process) will decrease the ARS adsorption rate at the second stage. The removal process was ordinary and 24 h of adsorption process was enough to reach an equilibrium.

Adsorption kinetics

The ARS adsorption kinetics was investigated with four theoretical models to describe the transport phenomena and the interaction between ARS and AC (Salam et al., 2014). The corresponding kinetic parameters from all models were listed in Table 2. The correlation between the experimental data and the theoretical data was evaluated by the different statistic coefficients (F_{cal}, R^2, and P value) described in the theoretical section.

Table 4 shows that pseudo-first order, external diffusion, and intra-particular diffusion models have a low value of R^2 (<0.94). In addition, a significant difference between the experimental and the calculated adsorption capacities observed for the three kinetic models. Previous studies have found similar behaviors during their investigation of the ARS adsorption by activated carbon. In fact, pseudo-first order, external diffusion, and intra-particular diffusion were not suitable for extracting kinetic parameters in agreement with other works (Fan et al. 2012; Kumar and Smaïl, 2010; Han et al. 2011; Crini 2008).

There is a good correlation between experimental values and of the calculation for the pseudo-second order kinetic model. Indeed, the correlation coefficient R^2 is 0.988 and there is good statistical signification (P value ≈ 0). Therefore, the pseudo-second order model is the suitable kinetic model that represents the kinetic adsorption of ARS on the elaborated AC. K_2 (constant of the pseudo-second order model) was the

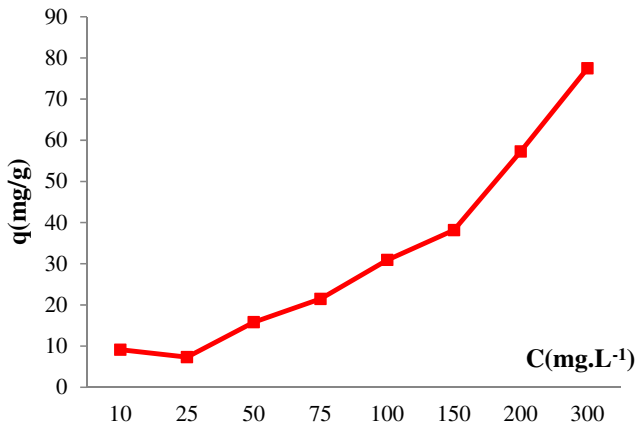

Fig. 8 Effect of initial concentration on the adsorption capacity (25 °C, pH 3, 1440 h)

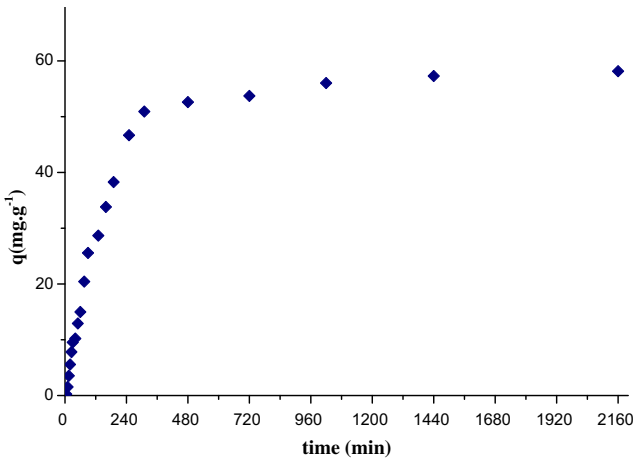

Fig. 9 Effect of contact time on the adsorption capacity (Ci 200 mg.L^{-1}, T 25 °C, pH 3)

Table 4 Kinetic parameters of ARS adsorption

Kinetic model	Model parameters	R^2	F_{cal}	P value	
Pseudo-first order	q_e (mg.g^{-1}) 47.9	K_1(min^{-1}) 0.009	0.932	232.2	2.41 10^{-11}
Pseudo-second order	q_e (mg.g^{-1}) 62.9	K_2(L.mg^{-1}.min^{-1}) 13 10^{-5}	0.988	1283.8	1.11 10^{-16}
External diffusion	K'(mg.g^{-1}.min$^{-0.5}$) 39 10^{-4}		0.932	233.4	2.32 10^{-11}
Intra-particular diffusion	K_{id}(mg.g^{-1}.min$^{-0.5}$) 6.228	C 25.1 10^{-3}	0.932	248.9	5.52 10^{-12}

adsorption reaction time-scaling factor. A low value of K_2 (K_2 = 13 10^{-5}) (L.mg^{-1}.min^{-1}) leads to a large time that is required to reach an equilibrium (Plazinski et al., 2013). The chemical adsorption promoted by the exchange of electrons between ARS and the adsorbent generates a valence liaison between adsorbent linking ARS and AC adsorbent. Similar results showing an applicability of the pseudo-second order model represent the kinetic adsorption of ARS by Ravindra et al. (2013).

The experimental kinetic adsorption of ARS on AC is characterized by a sharp increase in the adsorbed capacity during the first 250 min, followed by a lower adsorption, which can be described by the Weber and Morris model (Weber and Morris, 1963). According to the Weber and Morris model (or intra-particle model Table 1.), the initial part of adsorption is connected to faster mass transfer of ARS through the boundary layer and adsorption on the AC surface. The second part of adsorption is connected to slow diffusion inside the pores of AC. The slope of the linear portion of q vs $t^{1/2}$ (Fig. 10.) gives the rate constant of intra-particle diffusion K_i which equals 0.258 (mg.g^{-1}.min$^{1/2}$). The intercept of the linear portion is high (46.913), which clearly shows that surface adsorption is predominant. Indeed, at 300 min, the surface adhesion is completed and the pore diffusion started. Firstly, the adsorption is dominated by surface adhesion and afterwards, the pore diffusion.

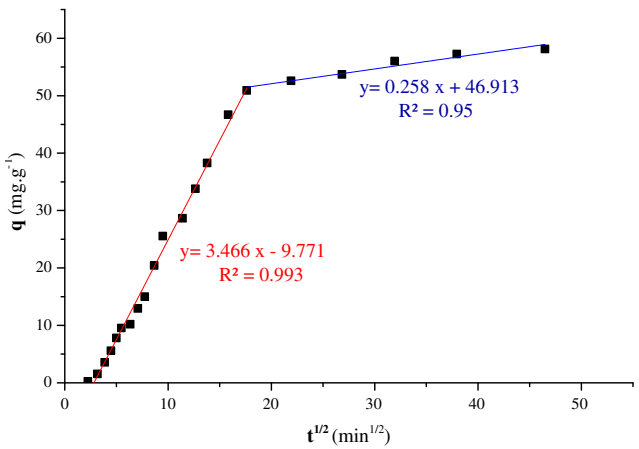

Fig. 10 Intraparticle plot for the adsorption of ARS

Adsorption isotherms

In order to understand the interaction nature between the AC and ARS, two- and three-parameter isotherm models were examined. Experimental data were fitted to each adsorption isotherm models and the most statistical significant model was used to describe the equilibrium adsorption.

Two-parameter isotherm

The first aim of this purpose was to find a two-parameter equation which can model the adsorption of ARS by AC in the range of ARS initial concentration between 5 and 300 mg.L^{-1}; controlled temperature was 25 °C; agitation was 200 rpm and pH 3. Three- and two-parameter models were used.

The Langmuir model is mainly used in the liquid phase adsorption and it is based on isotherm adsorption development involving two hypotheses. The first one is that the adsorbent has a limited adsorption capacity (q_{max}). The second one assumes only monolayer adsorption between adsorbent and solute (Langmuir 1918).

The Freundlich model is widely used as well in the modeling of liquid phase adsorption. It is applied, principally, in the multilayer adsorption isotherm where interactions between adsorbed molecules occurs (Freundlich 1906).

The Dubinin–Radushkevich model used in this study was in the liquid adsorption form. Three hypotheses correspond to this model. The first one is that the filling of the micropore volume is based on the fact that the adsorption potential is variable. The second assumes that the free adsorption enthalpy is related to the degree of pore filling. The third one considers that the surface of adsorbent was heterogeneous (Kennedy et al. 2007).

According to Table 5, the Langmuir model was the suitable model fitting well the ARS adsorption of on the elaborated AC. Indeed, the highest value of R^2 (0.988), the highest value

Table 5 Two-parameter isotherm models

Model	Parameters		R^2	F_{cal}	P value
Langmuir	q_m(mg.g^{-1}) 73.75	K_L(L.mg^{-1}) 0.023	0.988	1643	1.5 10^{-7}
Freundlich	K_f(mg$^{(1-n)}$.L^n.g^{-1}) 1.64	n 1.28	0.976	571.2	3.5 10^{-7}
Dubinin–Radushkevich	q_{mDR}(mg . g^{-1}) 1.1	E 0.874	0.762	22.4	2.1 10^{-3}

of F_{cal} (1643), and the lowest value of P (1.5 10^{-7}) reflect a statistical significance of this isotherm model.

The maximum adsorption capacity of ARS by AC determined by the mathematical model of Langmuir was about 73.75 mg.g^{-1}. The adsorption of ARS by AC was very favorable and probably a weakly reversible sorption. A previous work focused on the adsorption of ARS has also adapted the Langmuir isotherm as the best two-parameter model (Fadi and Bernard, 2009).

The Freundlich constant n was the characteristic of the adsorbate/adsorbent couple. If the value of n Freundlich is between 2 and 10, the adsorption is excellent, while if n is between 1 and 2, there is a good adsorption but if n is less than 1, the adsorption is low. The value of n obtained in this study is 1.28 which shows that the AC has good adsorbent capacity of ARS.

Compared with previous studies on ARS adsorption which are resumed in Table 6, the cotton-based activated carbon could be considered as a good adsorbent of ARS. The capacity of adsorption of ARS by AC was, relatively, acceptable despite the lower specific surface (292 m^2.g^{-1}. Table 4). This may suggest the involvement of the functional groups in the adsorption process which is more significant than the specific surface area effect. Indeed, chemical precipitations of the ARS anions/cations have a dominant responsibility in the adsorption capacity as was shown in a previous study (Albadarin and Mangwandi, 2015).

Three-parameter isotherm

Three two-parameter models were tested in order to improve the understanding of the ARS adsorption phenomena; three-parameter models were used. The most popular isotherm models with three parameters were investigated such as Redlich–Peterson, Tóth, Langmuir–Freundlich, Langmuir general, Sips, Radke–Prausnitz (1, 2, and 3), and Fritz–Schluender.

The Redlich–Peterson three-parameter model is the most widespread model in the literature. This model can be used for a wide concentration range. The equation of this model is a combination of the parameters of Langmuir and Freundlich. It is an empirical model combining the parameters of the Langmuir and Freundlich (Redlich and Peterson 1959).

The Tóth model is also often mentioned and applied. Basically, this model has been designed for the gas adsorption phase. Its empirical form is derived from the Langmuir model. This model considered that the surface of the adsorbent is energetically heterogeneous. The application of this model in the liquid phase is close to the empirical Redlich–Peterson model (Gimbert et al. 2008).

The Sips model is not used frequently in the literature. His mathematical expression was obtained by applying the mass action law. This model assumption is that the adsorption reaction stoichiometry would be in solute molecules per free adsorbent site (Sips 1948).

Table 6 Comparison of q_{max} of ARS with various adsorbents materials

Adsorbent	q_{max}(mg/g)	pH	C_i(mg/L)	T(°C)	ads $_{dosage}$ (g.L^{-1})	Reference
Activated carbon/γ-Fe_2O_3 nano-composite	108.7	2	150	25	1	(Fayazi et al. 2015)
Citrullus lanatus peels	79.6	3	100	30	5	(Fan et al. 2012)
Mustard husk	1.97	2–3	100	25	0.5	(Gautam et al. 2013)
Gold nanoparticles-AC	123.4	4.2	35	25	15	(Roosta et al. 2014)
Olive stone by-product	16.1	3.3	110	25	5	(Albadarin and Mangwandi 2015)
Magnetic chitosan	43.1	2–4	18	40	0.1	(Rehman and Mahmud 2013)
Cynodon dactylon	16.3	1	25	30	5	(Samusolomon and Devaprasath 2011)
Waste cotton-AC	73.8	2	300	25	0.5	This study

Table 7 Non-linear isotherm parameters

Model	n	K_L	q_m	R^2	F_{cal}	P value
Redlich–Peterson	0.162 ± 0.085	NA	0.728 ± 0.29	0.982	287.83	$1.1\ 10^{-6}$
Tóth	0.159 ± 0.103	NA	NA	0.982	287.83	$1.1\ 10^{-6}$
Langmuir–Freundlich	0.841 ± 0.24	NA	NA	0.982	287.83	$1.1\ 10^{-6}$
Langmuir general	0.841 ± 0.22	NA	NA	0.982	287.89	$1.1\ 10^{-6}$
Sips	0.842 ± 0.23	NA	NA	0.982	287.87	$1.1\ 10^{-6}$
Radke–Prausnitz 1	0.56 ± 0.21	NA	NA	0.989	433.40	$2.5\ 10^{-6}$
Radke–Prausnitz 2	0.139 ± 0.06	NA	0.647 ± 0.23	0.989	433.58	$2.5\ 10^{-6}$
Radke–Prausnitz 3	0.840 ± 0.76	NA	NA	0.982	287.92	$1.1\ 10^{-6}$
Fritz–Schluender	0.162 ± 0.06	0.729 ± 0.26	NA	0.982	287.82	$1.1\ 10^{-6}$

NA not applicable

Other three-parameter models were cited in previous studies and tested in this work such as Langmuir–Freundlich, Langmuir general, Radke–Prausnitz, and Fritz–Schluender model.

Firstly, these three-parameter models were tested using non-linear regression (Origin8.5. software). The obtained results are shown in Table 7.

Table 7 shows the application of isotherms in their non-linear form. The Redlich–Peterson, Radke–Prausnitz 2, and Fritz–Schluender models were relatively the best models that describe well the adsorption of ARS on the activated carbon ($R^2 > 0.98$ and P value ≈ 0). Langmuir–Freundlich, Langmuir general, Sips, and Radke–Prausnitz isotherm models are not adapted to describe the ARS adsorption. In spite of the similar values of "$n = 0.84$" for these models, there are aberrant values of K_L and q_m (sometimes negative values). In the case of a very high-standard error value, it can be concluded that the model is not relevant (exp: The model Radke–Prausnitz 3 is not relevant as $q_m = 484 \pm 3\ 10^6$).

The application of a non-linear three-parameter isotherm allowed the determination of n value for each model. The calculated n value was the following:

- n ≈ 0.16 for Redlich–Peterson, Tóth, and Fritz–Schluender isotherm
- n ≈ 0.84 for Langmuir–Freundlich, Langmuir general, Sips, and Radke–Prausnitz 3 isotherm
- n ≈ 0.56 for Radke–Prausnitz 1 isotherm
- n ≈ 0.14 for Radke–Prausnitz 2 isotherm

Unlike to the non-linear isotherm models with three parameters, it can be seen in Table 9 that Langmuir–Freundlich, Langmuir general, and Sips models can describe the ARS adsorption isotherm in the linear form. The accord of the models with the experimental data is good as observed through the R^2, F_{cal}, and P value values (Table.8). In almost all cases, the best isotherm model was Langmuir–Freundlich with $R^2 = 0.989$, $F_{cal} = 569$, and P value was near 0.

On the other hand, the isothermals Tóth, Radke–Prausnitz 1, 2, and 3, and Fritz–Schluender cannot be applicable to the adsorption of Alizarin S in their linear form because R^2 values are less than 0.89.

To have more than one three-parameter model that can describe the ARS adsorption by AC adsorption may be explained by the existence of two types of active sites on the surface of the AC. High-reactive sites, called sites 1, are

Table 8 Linear isotherm parameters

Model	n	K_L	q_m	R^2	F_{cal}	P value
Redlich–Peterson	0.16	NA	NA	0.846	38.43	$4.5\ 10^{-4}$
Tóth	0.16	5.95E-6	307,751	0.894	28.88	$17\ 10^{-4}$
Langmuir–Freundlich	0.84	0.0014	250	0.989	569.88	$3.5\ 10^{-7}$
Langmuir general	0.84	0.016	18.01	0.982	324.36	$1.9\ 10^{-6}$
Sips	0.84	0.003	232.56	0.989	569.88	$3.5\ 10^{-7}$
Radke–Prausnitz 1	0.56	0.697	0.767	0.642	12.53	$95\ 10^{-4}$
Radke–Prausnitz 2	0.14	NA	0.367	0.851	39.92	$3.9\ 10^{-4}$
Radke–Prausnitz 3	0.84	NA	NA	0.846	38.43	$4.5\ 10^{-4}$
Fritz–Schluender	0.16	0.454	NA	0.846	38.43	$4.5\ 10^{-4}$

NA not applicable

faintly distributed at the surface of the AC which reacted quickly with ARS even at low concentrations. Whereas, weakly active sites, called sites 2, highly distributed at the surface of the AC. Sites 2 react with the ARS after the saturation of the sites 1.

Redlich–Peterson, Radke–Prausnitz 2, and the Fritz–Schluender models would best model the ARS adsorption equilibrium in the non-linear form. However, Langmuir general and Sips models can describe the ARS adsorption isotherm in the linear form. This type of liquid phase adsorption was obtained by other researchers who have studied the application of three-parameter models with the linear and non-linear form (Mardini and Legube 2009).

A statistical approach was used to validate the isotherm model such as R^2, F_{cal}, and P value. In the first step, Langmuir model was adopted as the best two-parameter model that describes the adsorption of ARS by AC. In the second step, the model of Langmuir–Freundlich and Sips has been validated as the best three-parameter model which describes this type of adsorption.

Conclusion

The present investigation demonstrated the suitability of recycling cotton fiber for the preparation of activated carbon. The characterization of the activated carbon shows different types of functional groups especially basic groups such as the hydroxyl group on the surface of the AC. The AC presents mainly a microporous texture with uniform pores centered around 1 nm and some pores with sizes higher than 2 nm.

The ARS adsorption process by AC was found to depend on initial ARS concentration, pH, contact time, and temperature. A comparison of three kinetics models on the ARS adsorption shows that ARS/adsorbent reaction was best fitted by the pseudo-second order model. The adsorption data described well the Langmuir isotherm as a two-parameter model and Langmuir–Freundlich, Langmuir general, and Sips models as three-parameter models. Therefore, it was demonstrated that the AC derived from cotton waste could be used as an ARS adsorbent for textile wastewater. Future work on ARS adsorption will focus on the study of competition with complex molecules which exist in textile wastewater.

References

Albadarin AB, Mangwandi C (2015) Mechanisms of Alizarin Red S and methylene blue biosorption onto olive stone by-product: isotherm study in single and binary systems. J Environ Manag 164:86–93

Ali M, Courtenay P (2014) Evaluating the progress of the UK's material recycling facilities: a mini review. Waste Manag Res 12:1149–1157

Almasian A, Olya ME, Mahmoodi NM (2015) Synthesis of polyacrylonitrile/polyamidoamine composite nanofibers using electrospinning technique and their dye removal capacity. J Taiwan Inst Chem Eng 49:119–128

Altıntıg E, Arabacı G, Altundag H (2016) Preparation and characterization of the antibacterial efficiency of silver loaded activated carbon from corncobs. Surface & Coatings Technology. doi:10.1016/j.surfcoat.2016.06.077

Antal MJ (1984) Biomass pyrolysis, in K.W. Boer and J.A. Duffy (Eds.). Advances in Solar Energy. (3), 175–255

Azquez BL, Calero G, Ronda M, Tenorio A, Martín-Lara G (2014) Study of kinetics in the biosorption of lead onto native and chemically treated olive stone. J Ind Eng Chem 20:2754–2760

Bazrafshan A, hajati S, Ghaedi M (2015) Regenerable Zn(OH)2 nanoparticle-loaded activated carbon for the ultrasound-assisted removal of malachite green. Optimization, isotherm and kinetics, RSC Adv 5:79119–79128

Belhechemi M, Jeguirim M, Limousy L, Addoun F (2014) Comparison of NO_2 removal using date pits activated carbon and modified commercialized activated carbon via different preparation methods: effect of porosity and surface chemistry. Chem Eng J 253:121–129

Ben Hamissa AM, Lodi A, Seffen M, Finocchio E, Botter R, Converti A (2010) Sorption of Cd(II) and Pb(II) from aqueous solutions onto *Agave americana* fibers. Chem Eng J 159:67–74

Crini G (2008) Kinetic and equilibrium studies on the removal of cationic dyes from aqueous solution by adsorption onto a cyclodextrin polymer. Dyes Pigments 77:415–426

Dongqing Z, Jinxue L, Zarraz MP, Richard M, Yu L, Soon K, Wun JN (2016) Characterization of microbial communities in wetland mesocosms receiving caffeine-enriched wastewater. Environ Sci Pollut Res 23:1–14

Dubinin MM (1960) The potential theory of adsorption of gases and vapors for adsorbents with energetically nonuniform surfaces. Chem Rev 60:235–241

Ekrami E, Dadashian F, Soleimani M (2014) Waste cotton fibers based activated carbon: optimization of process and product characterization. Fibers and Polymers 15:1855–1864

Fadi AM, Bernard L (2009) Effect of the adsorbate (Bromacil) equilibrium concentration in water on its adsorption on powdered activated carbon. Part 2: kinetic parameters. J Hazard Mater 170:754–762

Fan L, Zhang y, Li X, Luo L, Lu F, Qiu H (2012) Removal of Alizarin Red from water environment using magnetic chitosan with Alizarin Red as imprinted molecules. Colloids Surf B: Biointerfaces 91:250–257

Fayazi M, Ghanei-Motlagh M, Taher MA (2015) The adsorption of basic dye (Alizarin Red S) from aqueous solution onto activated carbon-Fe2O3 nano-composite: kinetic and equilibrium studies. Mater Sci Semicond Process 40:35–43

Foo KY, Hameed BH (2010) An overview of dye removal via activated carbon adsorption process. Desalin and Water Treat 19:255–274

Freundlich H (1906) Over the adsorption in solution. Z Phys Chem 57: 384–470

Fritz W, Schluender EU (1974) Simultaneous adsorption equilibrium of organic solutes in dilute aqueous solution on activated carbon. Journal of Chemical Engineering Science 29:279–1282

Gautam RK, Mudhoo A, Chattopadhyaya MC (2013) Kinetic, equilibrium, thermodynamic studies and spectroscopic analysis of Alizarin Red S removal by mustard husk. J Environ Chem Eng 1:1283–1291

Ghouma I, Jeguirim M, Dorge S, Limousy L, Matei GC, Ouederni A (2015) Activated carbon prepared by physical activation of olive stones for the removal of NO2 at ambient temperature. Comptes Rendus Chimie 18:63–74

Gimbert F, Crini NM, Renault F, Badot PM, Crini G (2008) Adsorption isotherm models for dye removal by cationized starch-based

material in a single component system: error analysis. J Hazard Mater 157:34–46
Guo YP, Rockstraw DA (2006) Physical and chemical properties of carbons synthesized from xylan, cellulose, and Kraft lignin by H3PO4 activation. Carbon 44:1464–1475
Gupta VK, Suhas (2009) Application of low-cost adsorbents for dye removal—a review. J Environ Manag 90:2313–2342
Gupta VK, Gupta b, Rastogi A, Agarwal S, Nayak A (2011) A comparative investigation on adsorption performances of mesoporous activated carbon prepared from waste rubber tire and activated carbon for a hazardous azo dye–Acid Blue 113. J Hazard Mater 186:891–901
Gurudatt K, Tripathi VS, Sen AK (1999) Adsorbent carbon fabrics: new generation armour for toxic chemicals. Def Sci J 47:239–250
Han X, Wang W, Ma X (2011) Adsorption characteristics of methylene blue onto low cost biomass material lotus leaf. Chem Eng J 171:1–8
Haule LV, Carr MC, Rigout M (2014) Investigation into the removal of an easy-care crosslinking agent from cotton and the subsequent regeneration of lyocell-type fibres. Cellulose 21(3):2147–2156
Haule LV, Carr CM, Rigout M (2016) Investigation into the supramolecular properties of fibres regenerated from cotton based waste garments. Carbohydr Polym 144:131–139
Hinz C (2001) Description of sorption data with isotherm equations. Geoderma 99:225–243
Ho YS, McKay G (1999) Pseudo-second order model for sorption processes. Process Biochem 34:451–465
Javad Z, Neda A, Maryam B, Gholamhasan A (2014) Multi-response optimization using Taguchi design and principle component analysis for removing binary mixture of alizarin red and alizarin yellow from aqueous solution by nano c-alumina. Spectrochim Acta A Mol Biomol Spectrosc 126:291–300
Jie C, Xunwen S, Canhui L, Zehang Z, Xinxing Z, Guiping Y (2016) Water-soluble cellulose acetate from waste cotton fabrics and the aqueous processing of all-cellulose composites. Carbohydrate Polymers. In Press
Jieying Z, Quanlin Z, Zhengfang Y (2014) Preparation and characterization of activated carbon fiber (ACF) from cotton woven waste. Appl Surf Sci 299:86–91
Kennedy LJ, Vijaya JJ, Kayalvizhi K, Sekaran G (2007) Adsorption of phenol from aqueous solutions using mesoporous carbon prepared by two-stage process. Journal of Chemical Engineering 132:279–287
Kesraoui A, Moussa A, Ben Ali G, Seffen M (2015) Biosorption of alpacide blue from aqueous solution by lignocellulosic biomass: *Luffa cylindrica* fibers. Environmental Science and Pollution Research, 1–9
Koopal LK, van Riemsdijk WH, de Wit JCM, Benedetti MF (1994a) Analytical isotherm equations for multicomponent adsorption to heterogeneous surfaces. J Colloid Interface Sci 166:51–60
Kumar DB, Smaïl K (2010) Étude cinétique et thermodynamique de l'adsorption d'un colorant basique sur la sciure de Bois. Revue des sciences de l'eau Journal of Water Science 24:131–144
Lagergren S (1998) About the theory of so-called adsorption of soluble substances. K Svenska Vetenskapsakad Handl 24:1–39
Langmuir I (1918) The adsorption of gases on plane surfaces of glass, mica and platinum. J Am Chem Soc 40:1361–1403
Li FT, Yang H, Zhao Y, Xu R (2007) Novel modification pectin for heavy metal adsorption. Chin Chem Lett 18:325–328
Liang S, Guo X, Feng N, Tian Q (2010) Isotherms, kinetics and thermodynamic studies of adsorption of Cu2+ from aqueous solutions by Mg2+/K+ type orange peel adsorbent. J Hazard Mater 174:756–762
Liou TH (2010) Development of mesoporous structure and high adsorption capacity of biomass-based activated carbon by phosphoric acid and zinc chloride activation. Chem Eng J 158:129–142
Loelovich M (2008) Cellulose as a nanosructured polymer: a short review. Bioressources 3:1403–1418
Marchon B, Carrazza J, Heinemann H, Somorjai GA (1988) TPD and XPS studies of O_2, CO_2, and H_2O adsorption on clean polycrystalline graphite. Carbon 26:507–514
Mardini FA, Legube B (2009) Journal of hazardous materials. J Hazard Mater 170:744–753
Martynas T, Edvinas K, Viktoras R, Rainer H, Violeta K, Inga S, Dainius M (2013) Chemical degradation of various textile dyes as wastewater pollutants under dielectric barrier discharge plasma treatment. Engineering Journal 229:9–19
Mehrorang G, Sh H, Syamak NK, Reza S, Ali D, Behnaz B (2012) Comparison of silver and palladium nanoparticles loaded on activated carbon for efficient removal of methylene blue: kinetic and isotherm study of removal process. Powder Technol 228: 18–25
Nasiri Azad F, Ghaedi M, Ddashtian K, Montazerozohori M, Hajati S, Alipanahpour E (2015) Preparation and characterization of MWCNTs functionalized by N-(3-Nitrobenzylidene)-N′-trimethoxysilylpropyl-ethane-1, 2-diamine for the removal of aluminum (III) ions via complexation with ferrochrome cyanine R: spectrophotometric detection and optimization. RSC Adv 5:61060–61069
Ncibi MC, Mahjoub B, Seffen M (2006) Studies on the biosorption of textile dyes from aqueous solutions using *Posidonia oceanica* (L.) leaf sheath fibres. Adsorpt Sci Technol 24:461–473
Otake Y, Jenkins RG (1993) Characterization of oxygen-containing surface complexes created on a microporous carbon by air and nitric acid treatment. Carbon 31:109–121
Ouchi A, Toida T, Kumaresan S, Ando W, Kato J (2010) A new methodology to recycle polyester from fabric blends with cellulose. Cellulose 17:215–222
Parra S, Sarria V, Maloto, Periner P, Pulgarin C (2004) Photocatalytic degradation of atrazine using suspended and supported TiO_2 J. Appli Catal B: Environ 51:107–116
Pastor AC, Rodriguez-Reinoso F, Marsh H, Martinez MA (1999) Preparation of activated carbon cloths from viscous rayon. Part I. Carbonization procedures. Carbon 37:1275–1283
Pirillo S, Ferreiraa ML, Ruedaa EH (2009) The effect of pH in the adsorption of Alizarin and Eriochrome Blue Black R onto iron oxides. J Hazard Mater 168:168–178
Plazinski W, Dziuba J, Rudzinski W (2013) Modeling of sorption kinetics: the pseudo-second order equation and the sorbate intraparticle diffusivity. Journal of the international Adsorption society 19:1055–1064
Radke CJ, Prausnitz JM (1972) Adsorption of organic solutions from dilute aqueous solution on activated carbon. Ind Eng Chem Fundam 11:445–451
Ravindra KG, Ackmez M, Mahesh CC (2013) Kinetic, equilibrium, thermodynamic studies and spectroscopic analysis of Alizarin Red S removal by mustard husk. Journal of Environmental Chemical Engineering 4:1283–1291
Redlich O, Peterson DL (1959) A useful adsorption isotherm. J Phys Chem 57:1024–1031
Rehman R, Mahmud T (2013) Sorptive elimination of Alizarin Red-S dye from water using Citrullus lanatus peels in environmentally benign way along with equilibrium data modeling. Asian J Chem 25:5351–5356
Roosta M, Ghaedi M, Mohammadi M (2014) Removal of Alizarin Red S by gold nanoparticles loaded on activated carbon combined with ultrasound device: optimization by experimental design methodology. Powder Technol 267:134–144
Salam MA, El-Shishtawy RM, Obaid AY (2014) Synthesis of magnetic multi-walled carbon nanotubes/magnetite/ chitin magnetic nanocomposite for the removal of Rose bengal from real and model solution. J Ind Eng Chem 20:3559–3567

Samusolomon J, Devaprasath PM (2011) Removal of Alizarin Red S (dye) from aqueous media by using Cynodon dactylon as an adsorbent. J Chem Pharm Res 5:478–490

Sips R (1948) On the structure of a catalyst surface. J Chem Phys 16:490–495

Sylvie B, Nathalie A, Catherine B, Marie FP, Jose MLC, Olivier T (2005) Study of heterogeneous suspensions: a new quantitative approach coupling laser granulometry and UV–vis spectrophotometry. Colloids Surf A Physicochem Eng Asp 262:242–250

Tzvetkov G, Mihaylova S, Stoitchkova K, Tzvetkov P, Spassov T (2016) Mechanochemical and chemical activation of lignocellulosic material to prepare powdered activated carbons for adsorption applications. Powder Technol. doi:10.1016/j.powtec.2016.05.033

Wanassi B, Azzouz B, Ben-Hassen M (2016) Value-added waste cotton yarn: optimization of recycling process and spinning of reclaimed fibers. Ind Crop Prod 87:27–32

Weber WJ, Morris JC (1963) Kinetics of adsorption on carbon from solution. J Sanit Eng Div Am Soc Civ Engs 89:SA2–S31

Zaharia C, Suteu D (2012) Textile organic dyes-characteristics, polluting effects and separation/elimination procedures from industrial effluents—a critical overview. T. Puzyn (Ed.) Organic Pollutants Ten Years After the Stockholm Convention-Environmental and Analytical Update, InTech, Croatia, 472

Zahid M, Sabir H, Tanvir A, Habibullah N, Muhammad I, Azeem K, Muhammad A, Fabrice ML (2016) Use of RSM modeling for optimizing decolorization of simulated textile wastewater by *Pseudomonas aeruginosa* strain ZM130 capable of simultaneous removal of reactive dyes and hexavalent chromium. Environmental Science and Pollution Research. 1–16

Zainab ZI, Ali RT (2016) Recycled medical cotton industry waste as a source of biogas recovery. J Clean Prod 112:4413–4418

Zhuang Q-L, Kyotany T, Tomita A (1994) DRIFT and TK/TPD analyses of surface oxygen complexes formed during carbon gasification. Energy and Fuels 8:714–718